

An Assessment of Differences in Algorithms For Computing Fundamental Topographic Parameters

Su Jin Lee and Keith C. Clarke*

Department of Geography, University of California Santa Barbara.

[*kclarke@geog.ucsb.edu](mailto:kclarke@geog.ucsb.edu)

Abstract: The extraction of fundamental topographic parameters from digital elevation models (DEMs) is a common procedure in terrain analysis. Research to date has identified a set of derived parameters that in themselves are nearly complete descriptors of surface form, and that are highly correlated to surface structure. Different algorithms for calculating these fundamental topographic parameters from a DEM have been derived. Each makes assumptions about how surface properties should be calculated, and so produces different results when executed. This work assessed the method-derived differences among algorithms for computing fundamental topographic parameters. We used DEMs of 3m, 30m, and 90m resolutions covering Santa Barbara, CA. We assessed the quantity and location of the algorithmic differences between methods for computing aspect, slope, curvature, and flow. These were programmed from first principles into the MATLAB package. We analyzed aggregate surface mean, minimum, maximum, standard deviation, and variance. We also mapped the error, to characterize the magnitude of the differences in terms of terrain properties, and then examined them for scale dependences. The study permits conclusions about choice of method for the attainment of less overall, and more predictably located, error when terrain properties are computed for GIS-based terrain analyses.

KEYWORDS: Topography, digital elevation model, fundamental parameters, Matlab.

Introduction

An extraordinary amount of detailed data about the terrain surface of the earth has become available in the last few decades. The increasing availability of higher resolution and more timely digital elevation data force us to devote attention to terrain surface generalization. How can all of these DEMs be reduced from mere digits and map tiles to terrain constructs of use in the interpretation of the earth's form and its surface processes? The issue is not that of cartographic generalization, itself the source of volumes of research, but of terrain syntax and even semantics. For example, are there common shapes and forms into which all natural and human-made features on the earth's surface fall? The human mind can quickly reason from a contour loop with hachures to an enclosed depression and so to a karst sink-hole. The automated cartographic challenge is to have a computer follow the same detection-identification-explanation sequence as the trained geographer. The raw elevation data need to be automatically organized into features related to the land surface and its terrain structure, not structures imposed by data collection and storage. Only through building automated computational solutions to terrain abstraction can we deal with the rapidity with which new data can be captured.

To advance our knowledge of terrain syntax and semantics requires a comprehensive understanding of the fundamental parameters of topography (Evans, 1998). The fundamental parameters are the set of metric descriptors computable from any terrain data structure at any point on a surface that fully and completely describe the relations between that point and the overall surface. This includes both simple metrics, such as

derivatives, and the more complex terrain structure or skeleton, which may involve a recursive sub-division of the surface into line and area features such as slope facets, ridges, break-lines, and drainage features. A truly versatile terrain model would apply to all features on the earth's surface, be they large scale geomorphological, at the scale of the drainage basin, or influenced by human action and construction.

The fundamental topographic parameters should be computable from any of the GIS surface models: the square grid, the Triangulated Irregular Network, and the contour-based network (Wilson and Gallant, 2000), or indeed any possible surface abstraction. Nevertheless, the majority of the literature is heavily focused on the DEM and methods for computing from the grid. Moore et al. (1991) generated a list of parameters, which Wilson and Gallant (2000) summarized in a table. The table lists eighteen parameters: elevation, upslope height, aspect, slope, upslope slope, dispersal slope, catchment slope, upslope area, dispersal area, catchment area, specific catchment area, flow path length, upslope length, dispersal length, catchment length, profile curvature, plan curvature, tangential curvature, and elevation percentile. There is clearly correlation among these parameters, and we argue that elevation, slope, aspect, slope curvature, downslope direction and downslope accumulation are sufficient to characterize terrain. In and of themselves, these parameters are almost completely descriptive of surface form sufficient for a vast number of terrain analysis applications (Moore et al., 1991).

Yet agreement on which fundamental topographic parameters are indeed fundamental is trivial compared to differences created by what might be termed method-induced error. Wilson and Gallant's standardization of the formulae for the parameters (Wilson and Gallant, 2000), and the widespread availability of computer code for their computation through packages such as TAPES-G, have led to the incorporation of some or many of the parameters into GIS and other analytical software packages. However, the devil is often in the details, and the exact assumptions, computation methods, and handling of numerical error can make a huge difference in mapped and computed terrain values. The question posed in this study is: what differences in the computation of fundamental terrain parameters are the product of method-induced error, and how is that error manifested spatially, quantitatively and across spatial scales? Our goal is to sufficiently compute and describe the error for the same piece of terrain at three different spatial resolutions, to compare the computed parameters across methods, and to make recommendations about which algorithms to use to compute each parameter at different map scales. To implement this goal, we have coded selected algorithms from Wilson and Gallant (2000) in the MATLAB mathematical analysis package, and used the result to conduct an exhaustive cross-algorithm analysis for three nested DEMs.

In the following discussion, we start by reviewing prior work on the computation of fundamental topographic parameters, and then discuss the subset of methods that were implemented in MATLAB. A major computational challenge, the treatment of enclosed depressions by the algorithms, is discussed separately. We then describe the data sets used, and the results, analyzed across algorithm type (slope/aspect, slope curvature, and downslope measures) and by scale. The differences between the solutions are mapped for statistical and visual comparison, and conclusions are drawn. We conclude with a summary of recommendations for how to proceed with computing the fundamental topographic parameters from an unknown terrain sample at known scale and surface complexity.

Research on Topographic Structure

Terrain parameters such as slope gradient and orientation of slope (aspect) are important controls in many surface processes (Moore et al. 1993). O'Callaghan (1983) judged that the extraction of drainage networks from digital elevation data is critical for quantitative studies in geomorphology and hydrology, including sedimentary processes (Zevenbergen and Thorne, 1987). Early work on terrain description centered on the four topographic indices of slope, aspect, profile curvature and plan curvature (Evans, 1980). These topographic parameters are related to the central point of a 3 x 3 window within the DEM (Zevenbergen and Thorne, 1987). Douglas (1986) extended the research to develop methods to define ridges, channels, watersheds, and other hydrologic features from DEMs. Jenson and Domingue (1988) then devised methods to compute flow direction and flow accumulation. The flow direction for a cell is the direction in which water will flow out of the cell. It is encoded using a numbering convention to correspond with the center cell of a 3 x 3 neighborhood (figure 1). Speight (1974) described over twenty topographic attributes that can be used to describe the land surface form. A series of hydrologic topographic attributes was then adapted from the list (Speight 1974, 1980). Lea (1993) presented an aspect-driven kinematic routing algorithm. The algorithm is based on calculation of the aspect vector. This routing algorithm models flow moving kinematically from a point source at the center of the source pixel until it reaches a perimeter point on the cell boundary. In this study we adopted Lea's algorithm, but instead of a perimeter point we used a hollow point. In terms of tools for terrain analysis, Costa-Cabral and Burges presented the DEMON (Digital Elevation Model Networks) model (Costa-Cabral and Burges, 1994). Gallant and Wilson (1996) followed with TAPES-G, a grid-based terrain analysis program that computes slope, aspect, profile curvature, and plan curvature and several other topographic attributes for each cell of a squared-grid DEM. Wide availability of these tools has served to increase interest in and ability to compute measures of accuracy for terrain analysis algorithms.

Computing the Fundamental Parameters from DEMs

In the work reported on here, we chose to implement the computation of the fundamental topographic parameters from first principles, using formulae and heuristics described in the published literature rather than simply using one of the terrain analysis packages. To do so, we implemented the algorithms in MATLAB, a technical language for scientists. MATLAB is convenient for handling matrices, and DEMs have long been treated mathematically as matrices (Tobler, 1968). Prior to creating a simple ASCII file of elevations as {x, y, z} records of the array sizes listed in Table 2, however, the maps were reprojected to a common map projection and datum (NAD83 on UTM). We applied MATLAB programs that computed the fundamental topographic parameter using algorithms selected from Wilson and Gallant's list (Wilson and Gallant, 2000, p. 31). We chose three basic types of algorithm: slope and aspect, slope curvature, and downslope flow direction and accumulation.

Slope and Aspect Algorithms

Various slope and aspect algorithms are defined by the equations included in Table 1. In all cases, we refer to the gridded case and the simple 8-cell or Moore neighborhood, as shown in figure 1, with clockwise cell numbering that is unit indexed starting from the north-east.

Z7	Z8	Z1
Z6	Z9	Z2
Z5	Z4	Z3

Figure 1. 3 X 3 window showing cell numbering.

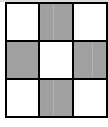
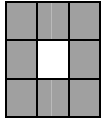
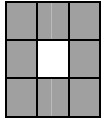
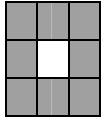
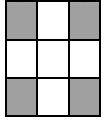
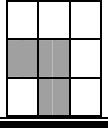
Topographic slope is the first derivative of elevation, given as the rise in elevation over the run in distance and obviously impacted by direction. In general, assuming angles clockwise from north in degrees, and Z_x representing east-west and Z_y representing north-south gradients:

$$Slope = \arctan(\sqrt{Z^2_x + Z^2_y}) \quad (\text{eq. 1})$$

$$Aspect = 180^\circ - \arctan\left(\frac{Z_y}{Z_x}\right) + 90^\circ \left(\frac{Z_x}{|Z_x|}\right) \quad (\text{eq. 2})$$

We define the horizontal resolution as h , and chose the following algorithms from the Wilson and Gallant list (Table 1). The algorithms are named using the Wilson and Gallant TAPES-G labels. Algorithm 2FD is the Second-order Finite Difference method (Fleming and Hoffer, 1979; Zevenbergen and Thorne, 1987; Ritter 1987). This algorithm deals only with the principal compass directions, and normalizes the slope vector between them. The 3FD algorithm is similar, termed the third-order Finite Difference (Sharpnack and Akin, 1969; Horn, 1981; Wood, 1996). This algorithm takes an average of the three vertical and horizontal cross vectors, ignoring the center grid cell in each case, and again normalizing the vector for X and Y. This algorithm is likely to be more smooth than 2FD, since it is an average over more samples. A modification of this method is the 3FDWRD or third-order Finite Difference Weighted by Reciprocal of Distance (Unwin, 1981). This method is the same as 3FD, but double-counts the vertical and horizontal profile running through the kernel cell, simulating a distance-decay effect. A further modification uses squared distance weighting, computing the third-order Finite Difference Weighted by Reciprocal of Squared Distance (3FDWRS) (Horn, 1981). This method weights the center by twice root 2 rather than the square. The far simpler FFD (Frame Finite Difference) method (Chu and Tsai, 1995) uses the cell corners rather than the kernel profiles, but otherwise resembles 2FD. Lastly, the SIMPLE Difference (SIMPLE D or SIMPLD) method (Jones, 1998) uses only a 4 cell neighborhood, looking only west and south and using only a single cell distance. This latter method is most sensitive to local variance, but similarly suffers a bias since the north and east cells slopes are not represented. In all cases, the slope and aspect solutions are yielded from equations (1) and (2).

Table 1. Formulae for slope and aspect computation from a DEM

		Zx	Zy
2FD		$z_x = \frac{(z_2 - z_6)}{2h}$	$z_y = \frac{(z_8 - z_4)}{2h}$
3FD		$z_x = \frac{(z_3 - z_5 + z_2 - z_6 + z_1 - z_7)}{6h}$	$z_y = \frac{(z_7 - z_5 + z_8 - z_4 + z_1 - z_3)}{6h}$
3FDWRD		$z_x = \frac{(z_3 - z_5 + 2(z_2 - z_6) + z_1 - z_7)}{8h}$	$z_y = \frac{(z_7 - z_5 + 2(z_8 - z_4) + z_1 - z_3)}{8h}$
3FDWRSD		$z_x = \frac{(z_3 - z_5 + 2\sqrt{z_2 - z_6} + z_1 - z_7)}{4 + 2\sqrt{2}}$	$z_y = \frac{(z_7 - z_5 + 2\sqrt{z_8 - z_4} + z_1 - z_3)}{4 + 2\sqrt{2}}$
3FFD		$z_x = \frac{(z_3 - z_5 + z_1 - z_7)}{4h}$	$z_y = \frac{(z_7 - z_5 + z_1 - z_3)}{4h}$
SIMPLD		$z_x = \frac{(z_9 - z_6)}{h}$	$z_y = \frac{(z_9 - z_4)}{h}$

A Note on Hollows and Flows

Various authors in terrain analysis have noted that “the horizontal and vertical resolution of most square-grid DEMs is such that that flow lines become trapped in pits and depressions (hollows) in key parts of the landscape” (Wilson and Gallant, 2000). Many proposed solutions have advocated preprocessing the DEM to eliminate these features (Jenson and Domingue, 1988; Hutchinson, 1989; Reiger, 1998). Hollows are represented by groups of cells whose aspects prevent downslope flow from escaping. This is illustrated by the three examples in figure 2. When constructing flow paths it is therefore necessary to record cells already in the flow path so that when hollows are reached, flow is prevented from moving indefinitely backwards or round and round (Lea,

1993). Typically, hollows are filled to the height of the next lowest cell in the eight-cell neighborhood, unless a more sophisticated tracking system is used.

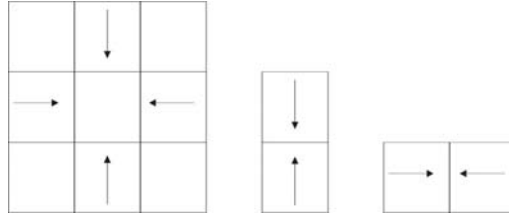


Figure 2. Typical hollow cases.

Curvature

Curvature attributes are based on second derivatives: the rate of change of a first derivative such as slope or aspect, usually in a particular direction. The two curvatures most frequently computed are plan (or contour) curvature, K_c , the rate of change of aspect along a contour, and profile curvature, K_p , the rate of change of slope down a flow line. Since profile curvature measures the rate of change of potential gradient, it is important for characterizing changes in flow velocity and sediment transport processes. Plan curvature measures topographic convergence and divergence and hence the propensity of water to converge as it flows across the land. Mitasova and Hofierka (1993) have suggested that tangential curvature, K_t (plan curvature multiplied by the sine of the slope angle), is more appropriate than plan curvature for studying flow convergence and divergence because it does not take on extremely large values when slope is small. The distribution of convex and concave area is the same for both plan and tangential curvature.

Formulae for the three curvature values are as follows:

$$K_p = \frac{Z_{xx}Z^2_x + 2Z_{xy}Z_xZ_y + Z_{yy}Z^2_y}{PQ^{3/2}} \quad (\text{eq. 3})$$

$$K_c = \frac{Z_{xx}Z^2_x - 2Z_{xy}Z_xZ_y + Z_{yy}Z^2_x}{PQ^{3/2}} \quad (\text{eq. 4})$$

$$K_t = \frac{Z_{xx}Z^2_x - 2Z_{xy}Z_xZ_y + Z_{yy}Z^2_x}{PQ^{1/2}} \quad (\text{eq. 5})$$

Using these formulae, profile curvature is negative for slope increasing downhill (convex flow profile, typically on upper slopes) and positive for slope decreasing downhill (concave, typically on lower slopes). Plan curvature is negative for diverging flow (on ridges) and positive for converging flow (in valleys) (Wilson & Gallant, 2000).

Downslope Flow

Flow is assumed to originate at the center of the source pixel and travel kinematically from a point source. Flow originates at the source point (SP: 2,2) and proceeds in the direction of the aspect (θ), until it reaches the next cell (Lea, 1993). For our purposes, we computed the flow direction and flow accumulation. Each of the downslope cells are affected by the aspect of the source cell, the source cell affects its adjacent rooks case neighbors (1,2), (2,3), (3,2), (2,1) as shaded zone in figure 3.

1,1	1,2	1,3
2,1	SP	2,3
3,1	3,2	3,3

Figure 3. 3 x 3 window for initial flow path from the center point of a pixel.

Flow within the source cell is assumed to travel from the cell center (the source point) to the outlet point (Xo,Yo). The outlet point (Xo,Yo) translates to an inlet point (Xi,Yi) on the perimeter of the neighboring pixel that shares the edge on each outlet point. If the aspect of the source pixel is 45°, 135°, 225°, or 315°, the outlet point has two adjacent cells. Flow directions and accumulations are constructed by the repeated application the algorithm. Figure 4. shows the diagram of the flow direction and flow accumulation.

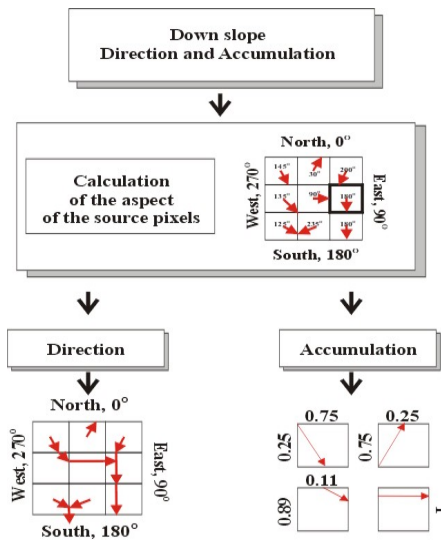


Figure 4. Flow chart of downslope flow: Direction and accumulation

The Multi-Resolution Test Data

As a test dataset we sought varied data at three spatial resolutions three orders of magnitude apart that reflected both steep and flatter terrain, and that were not devoid of typical DEM artifacts. We sought areas that varied from flat to steep, and with land uses from wildland to agriculture and urban. We were also aware of the precision effect on computed aspects noted by Carter (1992), and so treated all elevations as rounded integers. A search of the Santa Barbara, California region using the National Map viewer (<http://nmviewogc.cr.usgs.gov/viewer.htm>) led us to DEMs for the region at 30m from the National Elevation Database (composed of mosaiced seven-and-a-half-minute DEMs) and at 90m from the Shuttle Radar Topographic Mapping mission, both with one meter vertical precision. These were chosen to overlap an existing 3m DEM (with 2 ft. vertical resolution) obtained by detailed digitizing of topographic maps by Ed Keller and Mark De La Garza of the UCSB Department of Geological Sciences.

The overlapping areas chosen begin with the detailed 3m DEM, which covers only a small portion of Ellwood Canyon, just west of Goleta, California. This zone is an agricultural valley with areas of citrus orchards on flatter land and increasingly steep slopes covered by chaparral at the edge. Ellwood Canyon is one of several intermittent stream canyons draining the foothills of the Santa Ynez coastal range mountains, which rise to about 1200m. This is an east-west running range, and the study area covers the south facing slopes of approximately the center of the range. Zooming out to the 30m dataset includes both the neighboring canyons to the east and west, but also the peak regions along the ridge-following road, and the flatter urban and agricultural land of northern Goleta and unincorporated Santa Barbara County. At 90m, the region stretches from beyond the mountains into the Santa Ynez Valley through the San Marcos Pass, a saddle followed by the only major road to cross the mountains. The DEM at 90m includes the entire city of Goleta, the UCSB campus, the coastal plain and wetlands, the airport, and stretches to the ocean, in the south of the dataset. Figure 5 (a) shows the digital orthophoto coverage of the study area. Figure 5 (b) shows a hill-shaded rendition of the study area (Solar Azimuth 45°, Elevation 45°). In each figure, the orange box is the 3m resolution DEM, the green box is 30m resolution DEM, and the whole image is 90m resolution DEM. Table 2 lists the extent, size and resolution of the three data sets.

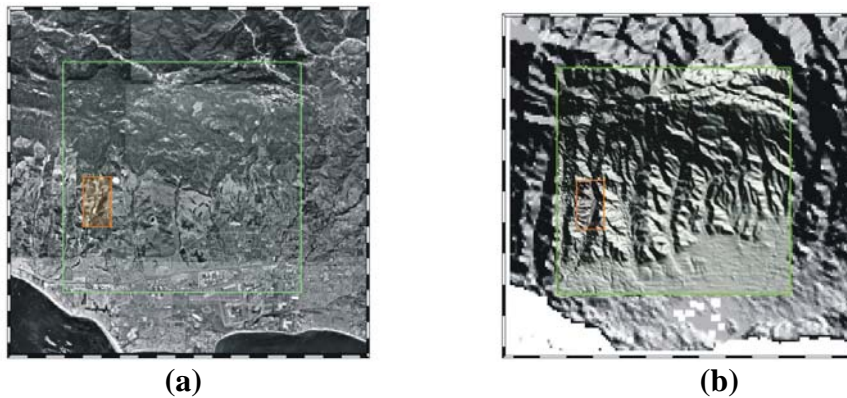


Figure 5. Digital Orthophoto and Hill-shaded DEM

Statistics describing the DEM elevation values were computed and are recorded in table 3. All units are in meters. Since the extents are different for the three different resolutions, the extremes and variances are not directly comparable. In the 3m DEM, elevations ranged from 50 to 215 m. The 30m and 90m DEMs both stretched from sea level to over 900m, zero elevations in the ocean were excluded from the computations. The mid-slope nature of the 3m DEM is obvious from the histograms of elevation shown in figure 6. In each case, elevations showed the characteristic exponential drop in frequency with elevation, with a secondary peak in the foothills of the mountains at about 700m. The 3m DEM was located further down the slope than this, and so has a far lower variance and elevation standard deviation.

Table 2. Extent of each DEM.

Resolution	Top left	Bottom right	Length	X cell	Y cell
3m	34 ° 28'16.89"N 119 ° 53'51.99"W	34 ° 27'14.64"N 119 ° 53'8.71"W	E-W: 1050 m N- S: 1950 m	350	650
30m	34 ° 30'41.58"N 119 ° 54'26.83"W	34 ° 25'57.99"N 119 ° 48'24.52"W	E-W: 9000 m N- S: 9000 m	300	300
90m	34 ° 31'49.63"N 119 ° 55'47.08"W	34 ° 24'44.23"N 119 ° 46'43.62"W	E-W: 13500 m N- S: 13500 m	150	150

Table 3. Descriptive statistics for each DEM (units are meters)

Resolution	Average	Median	Minimum	Maximum	Standard Deviation	Variance
3m	119.56	120.0	50.0	215.0	35.13	1234.30
30m	283.00	148.0	1.0	931.0	276.51	76452.76
90m	306.66	163.0	1.0	992.0	296.14	87699.79

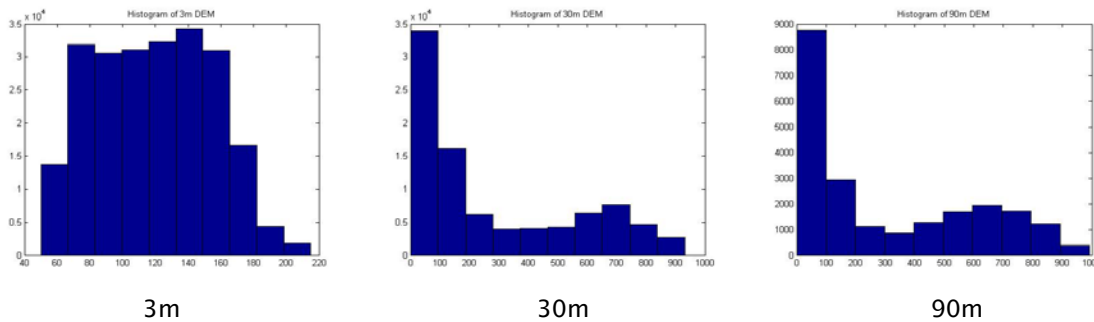


Figure 6. Histograms of elevation.

Results

The six methods used to calculate slope, aspect, curvature, and down slope were statistically compared with each value, using average (AVE), median (MED), minimum (MIN), maximum (MAX), standard deviation (STD), and variance (VAR). The below left figures show images from each of the 2FD, 3FD, 3FDWRD, 3FDWRSD, 3FFD, and SIMPLE D algorithms, and right figures are showing the statistical analysis AVE, MED, MAX, VAR, STD, and MIN, from top left clockwise.

Slope

In the slope case, the values of SIMPLE D method are significantly different with the others in all analysis and resolution. The minimum values of 3FD, 3FDWRD, and 3FDWRSD methods are comparatively less. Among those minimum values, 3FDWRD's is the most significant low value. Especially, only in the lowest resolution (90m), the 3FFD method distinguishes the results that the values of AVR, MED, MAX, STD, and VAR are apparently different from the others.

Table 4. Statistical analysis of Slope

	Resolution	2FD	3FD	3FDWRD	3FDWRS	3FFD	SIMPLE D
Average	3m	19.29	17.92	17.92	17.94	18.05	23.92
Median	3	18.43	16.66	17.12	16.72	14.76	18.43
Minimum	3	9.46	3.18	1.64	3.37	6.72	18.43
Maximum	3	77.67	76.81	76.88	77.00	76.99	80.04
Std. Dev.	3	8.84	9.03	9.06	9.11	8.97	8.10
Variance	3	78.08	81.50	82.14	83.04	80.49	65.69
Average	30	13.55	13.06	13.10	13.14	12.97	14.60
Median	30	12.60	12.21	12.23	12.26	12.05	13.52
Minimum	30	0.95	0.32	0.07	0.34	0.67	1.90
Maximum	30	50.65	46.83	47.08	47.63	46.94	54.47
Std. Dev.	30	9.42	9.26	9.29	9.31	9.18	9.65
Variance	30	88.74	85.82	86.22	86.66	84.26	93.05
Average	90	13.52	13.28	13.37	13.44	12.7302	14.31
Median	90	10.39	9.82	9.92	10.02	9.4338	11.24
Minimum	90	0.32	0.11	0.04	0.11	0.2250	0.64
Maximum	90	82.94	80.64	80.87	81.15	80.1483	86.45
Std. Dev.	90	15.53	15.38	15.44	15.52	15.0672	15.43
Variance	90	241.32	236.45	238.52	240.90	227.02	238.09

Aspect

In the aspect analysis, the SIMPLE D method shows a quite different result compared to the other methods. The 3FDWRD method makes the lowest minimum value in all the resolutions. Generally, the result trend of 3FD, 3FDWRD, 3FDWRS, and 3FFD are similar. Depending on resolution, there is no special trend save for the median value of 3m resolution.

Slope and aspect, the two most basic of the fundamental topographic parameters, show clearly that there is method-induced difference attributable to the various algorithms. In most cases, the 3FDWRD algorithm computed the lowest minimum value and had a high or the highest variance. The SIMPLE D algorithm consistently underestimated the values and showed structurally different comparative the results.

Plan curvature

Negative values of plan curvature show a divergence flow (e.g. on a ridge), and positive values represent convergent flow (e.g. in a canyon or valley). The 3FD (3m) and the 2FD (90m) method yielded quite different results compared to the other methods. This was not true of the 30m resolution, where all the results are similar. In Table 6, first of all, the plan curvature values for 3FD, 3FDWRD, 3FDWRS, and 3FFD are shown. According to these results, the 3FD, 3FDWRD, 3FDWRS, and 3FFD algorithms vary widely across the resolutions, but only minimally within each dataset.

Table 5. Statistical analysis of Aspect

	Resolution	2FD	3FD	3FDWRD	3FDWRSD	3FFD	SIMPLE D
Average	3m	193.85	196.39	196.38	196.41	195.53	181.88
Median	3	225.00	225.00	225.00	225.00	225.00	225.00
Minimum	3	3.81	2.49	0.86	1.74	3.81	7.13
Maximum	3	352.87	357.40	358.78	357.71	356.19	348.69
Std. Dev.	3	101.84	106.36	106.44	106.46	104.91	95.28
Variance	3	10371.71	11312.59	11329.83	11332.92	11005.13	9078.27
Average	30	189.17	189.00	188.93	188.93	189.12	188.31
Median	30	216.03	213.69	213.37	213.50	215.54	216.87
Minimum	30	1.19	0.39	0.035	0.29	0.61	2.05
Maximum	30	358.90	359.51	359.93	359.64	359.33	357.88
Std. Dev.	30	121.26	123.27	123.43	123.31	122.93	118.86
Variance	30	14702.90	15195.05	15234.50	15206.57	15111.23	14127.61
Average	90	184.35	183.84	183.96	184.05	183.46	180.20
Median	90	191.31	189.44	189.07	189.59	189.25	191.31
Minimum	90	0.0559	0.0189	0.0097	0.028	0.0279	0.056
Maximum	90	359.94	359.98	359.99	359.99	359.97	359.94
Std. Dev.	90	117.56	119.26	119.57	119.23	118.81	114.93
Variance	90	13819.62	14224.15	14297.94	14215.66	14116.04	13208.08

Table 6. Statistical analysis of Plan curvature

	Resolution	2FD	3FD	3FDWRD	3FDWRSD	3FFD	SIMPLE D
Average	3m	-0.0013	-0.001	-0.00107	-0.00106	-0.00106	0.00102
Median	3	0	0	0	0	0	0
Minimum	3	-1.53206	-2.14663	-4.85702	-2.35702	-1.64992	-2.33333
Maximum	3	2.66667	8	6.4379	5.33333	2.66667	2.33333
Std. Dev.	3	0.26217	0.29462	0.2931	0.29308	0.30756	0.18396
Variance	3	0.06873	0.0868	0.0859	0.08589	0.094593	0.03384
Average	30	0.00006	-0.00002	-0.00007	-0.00004	0.00001	0.00025
Median	30	0	0	0	0	0	0
Minimum	30	-1.03709	-2.46667	-4.45584	-4.57262	-1.15494	-0.43333
Maximum	30	1.06667	2.4	4.66274	3.91266	2.26667	0.80728
Std. Dev.	30	0.0337	0.04214	0.04783	0.0434	0.03851	0.02355
Variance	30	0.00113	0.00177	0.00228	0.00188	0.00148	0.00055
Average	90	-0.01914	-0.02969	-0.02798	-0.03014	-0.02802	-0.01377
Median	90	0	0	0	0	0	0
Minimum	90	-44.7111	-134.133	-134.297	-157.339	-78.6696	-11.1778
Maximum	90	44.48889	70.86388	41.17848	39.8676	63.28606	1.98972
Std. Dev.	90	1.185955	2.128928	1.889189	1.874926	1.652424	0.314503
Variance	90	1.406489	4.532333	3.569036	3.515346	2.730506	0.098912

Profile curvature

Profile curvature measures the rate of change of the potential gradient, and so is important for characterizing flow velocity and sediment transport. Using equation 4, profile curvature is negative for slopes increasing downhill (convex flow profile, typically on upper slopes), and positive for slopes decreasing downhill (concave, typically on lower slopes). Except for the 2FD (90m) result, most of the results seem

alike, and we can see the characteristic flow lines against a fairly uniform mean value. In the statistics, the minimum value of 3FDWRD (3m) alone is positive, and the other distributions are similar save for the SIMPLE D algorithm. For the 30m DEM, there is no significant difference between the algorithms. For the 90m DEM, the 3FD, 3FDWRD, and 3FDWRS D algorithms show apparent differences from the remainder, in particular that the average value of SIMPLE D is always negative.

Tangential curvature

Tangential curvature was suggested by Mitasova and Hofierka (1993) as more appropriate than plan curvature for studying flow convergence and divergence because it does not trend to extremes when the slope is small. The distribution of convex and concave area is the same for both plan and tangential curvature. Tangential curvature is curvature in an inclined plane perpendicular to both the direction of flow and the surface (Gallant and Wilson, 1996). Except for the 2FD algorithm (90m) and SIMPLE D (3m), most of the results seem to be similar. In the statistical analysis of the 3m and 30m DEMs, the average values of SIMPLE D are positive. For the 90m DEM, the 2FD algorithm computed quiet different average and minimum values. As before, 3FD, 3FDWRD, and 3FDWRS D have similar values.

Table 7. Statistical analysis of Profile curvature

	Resolution	2FD	3FD	3FDWRD	3FDWRS D	3FFD	SIMPLE D
Average	3	0.00019	0.00018	0.00019	0.00019	0.00011	0.00169
Median	3	0	0	0	0	0	0
Minimum	3	-0.32911	-0.34043	0.34106	-0.33603	-0.34482	-0.55505
Maximum	3	0.38848	0.45607	0.4501	0.43534	0.45712	0.94868
Std. Dev.	3	0.07779	0.07766	0.07792	0.07813	0.07608	0.06015
Variance	3	0.00605	0.00603	0.00607	0.0061	0.00578	0.00361
Average	30	0.00006	0.00006	0.00006	0.00006	0.00006	0.00008
Median	30	0	0	0	0	0	0
Minimum	30	-0.04306	-0.04641	-0.04605	-0.04558	-0.0464	-0.03628
Maximum	30	0.04558	0.04622	0.04638	0.04648	0.04529	0.04323
Std. Dev.	30	0.003578	0.003586	0.003588	0.003591	0.00357	0.003549
Variance	30	1.28E-05	1.29E-05	1.29E-05	1.29E-05	1.27E-05	1.26E-05
Average	90	0.00041	0.00011	0.00011	0.00013	0.00027	-0.00038
Median	90	0	0.00001	0.00001	0.00001	0	0
Minimum	90	-0.06231	-0.24863	-0.19422	-0.24716	-0.18555	-0.18558
Maximum	90	0.27903	0.26039	0.26242	0.26217	0.24834	0.04246
Std. Dev.	90	0.010432	0.007795	0.007224	0.007297	0.01205019	0.0070469
Variance	90	0.000109	6.08E-05	5.22E-05	5.325E-05	0.00014520	4.965E-05

Down Slope Accumulation

We calculated down slope parameters using down slope accumulation and down slope direction. In the accumulation map, flow lines are dark blue. These flow lines show streams closely in the 30m and 90m DEM. Also the high resolution, 3m DEM shows a stream line in the valley bottom. It is hard to find high convergence in the 3m DEM, but it shows clearly in the canyons in the 30m and 90m DEMs. In these analyses, generally

Table 8. Statistical analysis of Tangential curvature

	Resolution	2FD	3FD	3FDWRD	3FDWRSD	3FFD	SIMPLE D
Average	3m	-0.00005	-0.00002	-0.00002	-0.00001	-0.00006	0.00789
Median	3	0	0	0	0	0	0
Minimum	3	-0.72748	-0.77742	-0.77369	-0.76891	-0.78378	-0.94868
Maximum	3	0.85408	0.92897	0.92187	0.91331	0.94898	1.79196
Std. Dev.	3	0.09123	0.09658	0.09582	0.095	0.09843	0.08711
Variance	3	0.00832	0.00932	0.00918	0.00902	0.00968	0.00758
Average	30	-0.00004	-0.00003	-0.00003	-0.00003	-0.00002	0.0001
Median	30	0	0	0	0	0	0
Minimum	30	-0.06994	-0.06888	-0.0698	-0.07042	-0.06621	-0.04666
Maximum	30	0.08503	0.08079	0.08188	0.08282	0.07574	0.06536
Std. Dev.	30	0.004732	0.004795	0.004791	0.004782	0.004796	0.004558
Variance	30	2.24E-05	2.3E-05	2.29E-05	2.29E-05	2.3E-05	2.08E-05
Average	90	0.00153	0.00006	0.00004	0.00005	-0.00019	-0.00037
Median	90	0	0	0	0	0	0
Minimum	90	0	-0.30971	-0.30971	-0.349	-0.3097	-0.24801
Maximum	90	0.13037	0.44562	0.42716	0.4327	0.49505	0.03361
Std. Dev.	90	0.00926	0.013051	0.012639	0.012356	0.013469	0.008237
Variance	90	8.58E-05	0.00017	0.00016	0.000153	0.000181	6.79E-05

Table 9. Statistical analysis of Down slope accumulation

	Resolution	2FD	3FD	3FDWRD	3FDWRSD	3FFD	SIMPLE D
Average	3m	0.916044	0.931565	0.930207	0.930466	0.948356	0.782163
Median	3	0.91667	0.975	0.98223	0.97368	1	0.5
Minimum	3	0	0	0	0	0	0
Maximum	3	4.5	4.5	4.5	4.5	4.5	4.75
Std. Dev.	3	0.758103	0.551382	0.549287	0.553524	0.630442	0.878001
Variance	3	0.57472	0.304023	0.301716	0.306389	0.397457	0.770886
Average	30	0.931256	0.952056	0.9507	0.951567	0.948556	0.903422
Median	30	0.93452	0.95455	0.95669	0.95555	0.95455	0.90476
Minimum	30	0	0	0	0	0	0
Maximum	30	5.875	5.73333	5.76776	5.80357	5.66666	5.41667
Std. Dev.	30	0.614504	0.526282	0.519127	0.527487	0.530336	0.667133
Variance	30	0.377615	0.276973	0.269493	0.278242	0.281257	0.445066
Average	90	0.955378	0.9684	0.969511	0.967956	0.962622	0.968
Median	90	0.904765	0.932895	0.93934	0.93394	0.92857	0.875
Minimum	90	0	0	0	0	0	0
Maximum	90	5.625	5.14167	5.26429	5.38333	5.36667	5.0015
Std. Dev.	90	0.722315	0.628034	0.61547	0.634062	0.60946	0.775872
Variance	90	0.521739	0.394426	0.378803	0.402034	0.371442	0.601978

the results of 3FD, 3FDWRD, 3FDWRSD, and 3FFD algorithms seem to be similar. We conclude from the accumulation analysis that at all three scales down slope accumulation represents converging water flow better than down slope direction.

Summary

The statistical tabulation of fundamental topographic properties computed across scales using the various algorithms has shown that there is indeed statistically significant

method-produced error in the algorithms, and that this error is some function of scale, although not in all cases. This does not, however, answer the question of where the differences are manifested within the DEM. In the following section, we seek to map the algorithmic differences, and to assess what elements are present about which general recommendations might be made.

Spatial Distributions of Algorithmic Difference

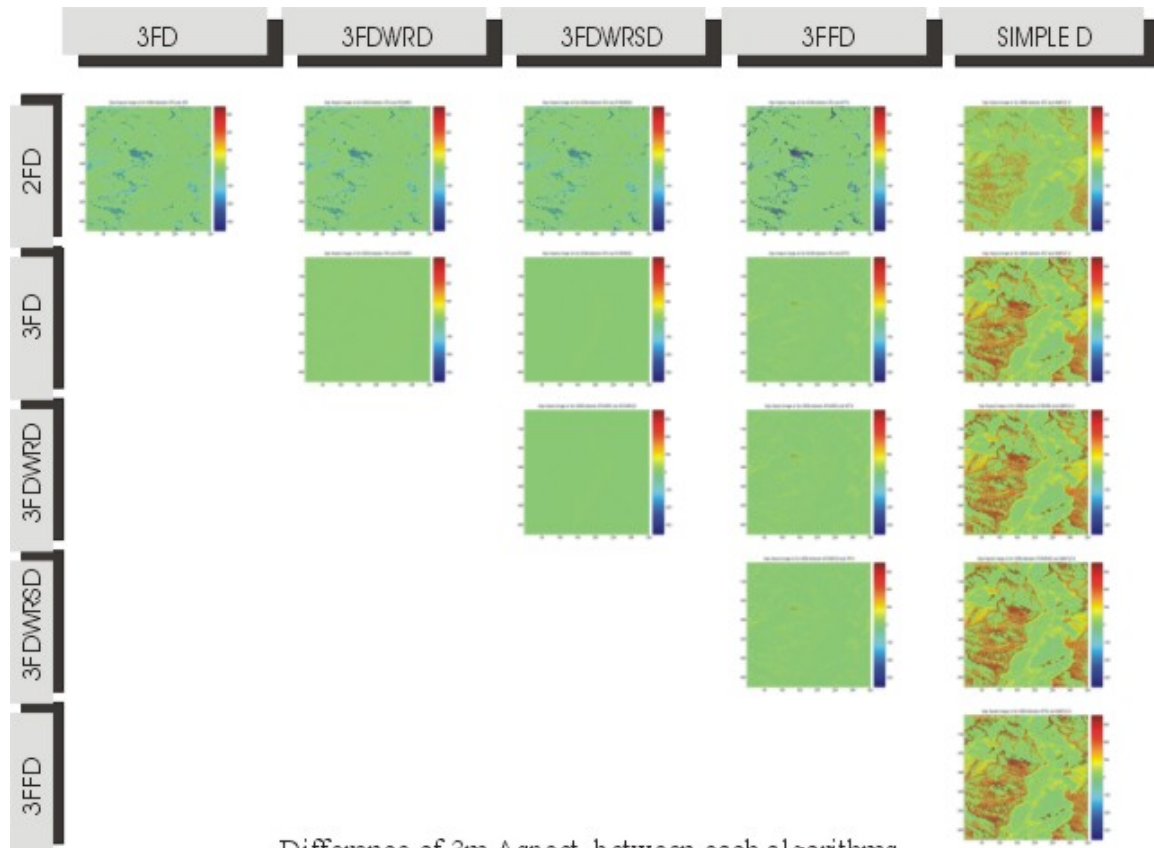
We computed the paired differences for the three DEMs between all combinations and permutations of algorithms. With three resolutions and five fundamental parameters, the results are too many to show in this paper. We have selected, therefore only two instances that show maximal method-produced difference. Figure 7 and 8 show two examples, the 3m data sets for each algorithm for two parameters. In each case only one half of the pair-comparison matrix is shown since they are symmetrical about the leading diagonal, with only the sign changed. In the two figures, the axis of each figure is the same size, therefore different colors represents the differences between each pair of algorithms. Green is at the center of the scale, corresponding to no difference between algorithms.

Table 10. Statistical analysis of Down slope direction

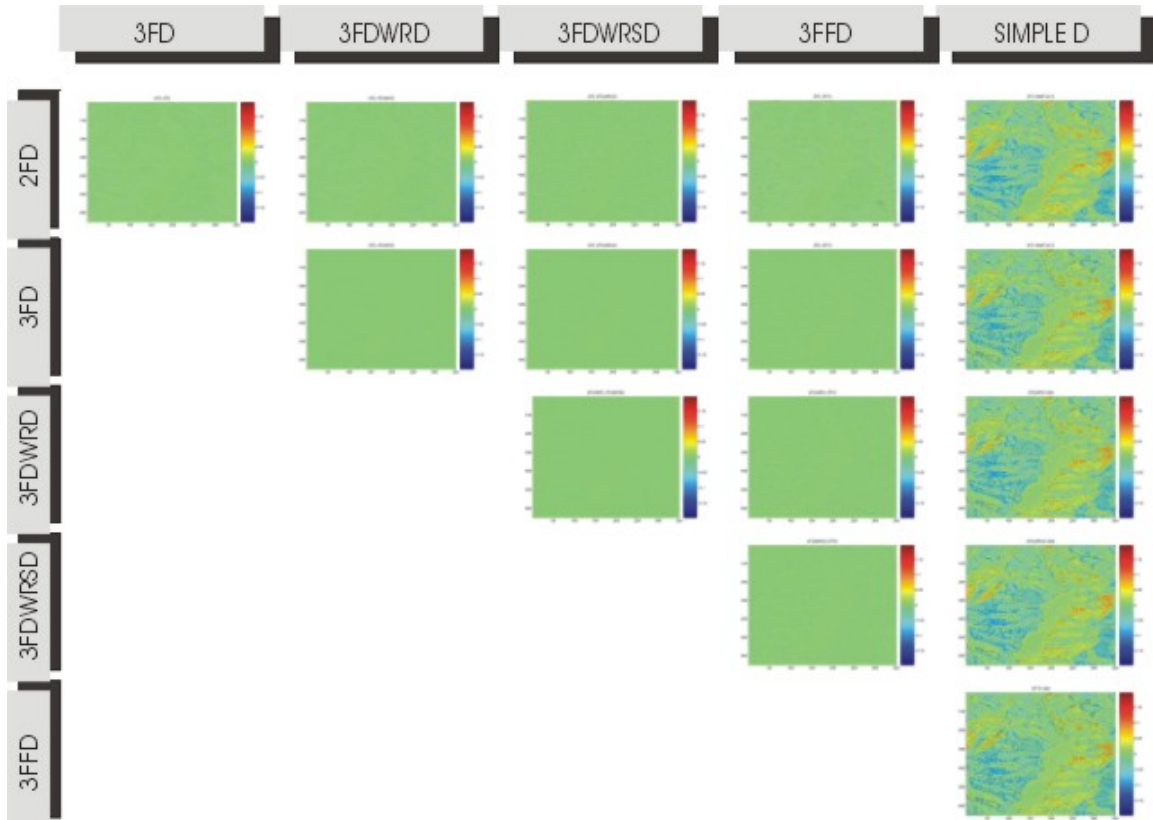
	Resolution	2FD	3FD	3FDWRD	3FDWRS	3FFD	SIMPLE D
Average	3m	11.1493	13.34403	13.37593	13.41589	12.83983	4.743477
Median	3	2	3	4	4	4	1
Minimum	3	0	0	0	0	0	0
Maximum	3	4363	4068	4067	4087	4430	1491
Std. Dev.	3	60.21325	68.53191	68.60219	68.86897	63.35333	22.68011
Variance	3	3625.636	4696.623	4706.261	4742.935	4013.644	514.3874
Average	30	13.15108	13.70862	14.00507	13.83769	14.08023	12.16021
Median	30	3	4	4	4	4	3
Minimum	30	0	0	0	0	0	0
Maximum	30	1479	1582	1458	1458	1335	1075
Std. Dev.	30	47.86049	49.65852	52.59124	51.19556	49.28985	40.36706
Variance	30	2290.627	2465.969	2765.838	2620.986	2429.49	1629.499
Average	90	7.213511	7.625244	7.548978	7.398356	8.111422	6.049822
Median	90	2	3	3	3	3	2
Minimum	90	0	0	0	0	0	0
Maximum	90	509	375	374	360	555	307
Std. Dev.	90	18.44081	18.97207	18.63233	17.47034	23.32765	14.19683
Variance	90	340.0636	359.9396	347.1637	305.2129	544.1791	201.55

Figure 7 (3m) shows the values for aspect computed with the six algorithms. Of these, the greatest variations in results are between SIMPLE D and 2FD versus the remainder, which are comparable. The differences are most striking at the highest resolution, but are similar in structure at the other two scales. The 2FD differences are negative (i.e. 2FD overestimates aspect) although the differences are minor. SIMPLE D in all cases underestimates aspect, it tends to smooth and oversimplify the surface. This is more the case at north and south-facing slopes, implying quantization error at 180 and 360 degrees. It is also the highest on steeper slopes and at higher elevations.

A similar result is the case for considering Tangential curvature at 3m (Figure 8). Again, by far the majority of differences are between the SIMPLE D method and all others. This effect is also mitigated by scale, i.e. differences are highest at 3m and diminish with smoothing to 30 and 90m. In this case, the difference in Tangential curvature between any of the other methods and SIMPLE D was both positive and negative, and remarkably consistent. There is apparently a strong correlation with aspect error, note that the blues and reds in figure 8 match the browns and yellows in figure 7 respectively quite well. This plan curvature error in SIMPLE D seems derivative of the fact that SIMPLE D does a relatively poor job of computing terrain aspect, especially in the principal compass directions.



Difference of 3m Aspect between each algorithms
Figure 7. Difference of aspect



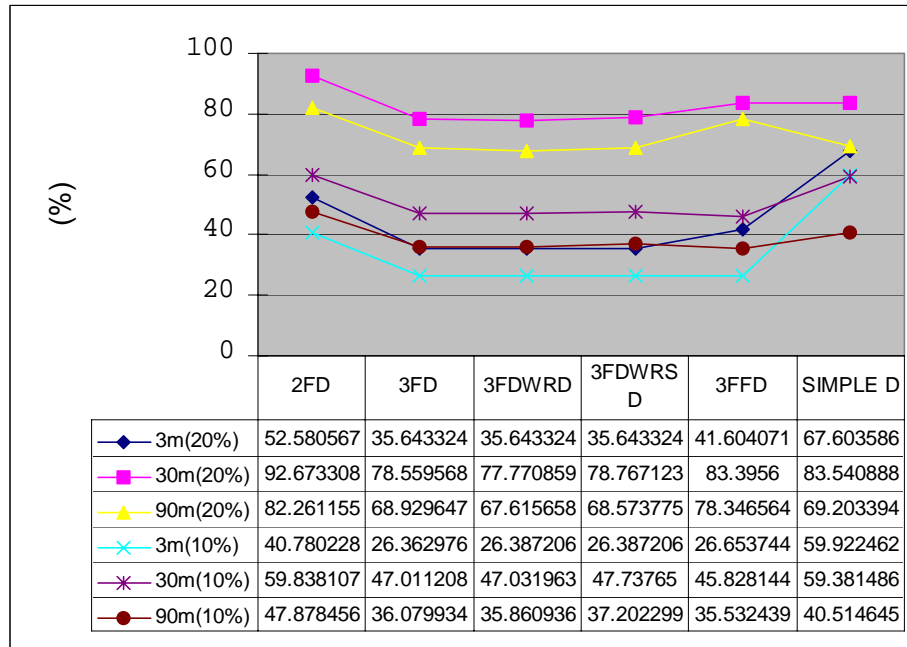
Difference of Tangential curvature of 3m DEM
 Figure 8. Difference of Tangential curvature

Error and Stream Flow

We compared the different algorithms' abilities to enhance the stream network by comparing the down slope accumulation data with digitized stream symbols extracted from the National Map, these derived from the blue lines of seven-and-a-half minute 1:24,000 map quadrangles. Almost all streams in this area are ephemeral. In the case of the down slope accumulation, both 10% and 20% thresholds (of all pixels) were used to distinguish between cells likely to contain streams and those not likely. As before, these are shown at the three spatial resolutions and extents. In each case there is a very close degree of correspondence between the highest values of the down slope accumulation ratio and the digitized stream network. There is a noticeable one pixel offset to the south and east, most likely reflecting the pixel processing order in the algorithms. Such an effect could be easily compensated for in actual systems. Overlay of the digital map stream pixels with the thresholded down slope flow accumulation images creates a map of correct/incorrect assignments of pixels to streams. The values shown are the percentage of pixels that fall into the digitized stream lines as a proportion of all stream line pixels, comparable to a percent-correct accuracy measure (Table 11). This allows an accuracy assessment of sorts, although the digital map versions of the streams could be significantly improved by detailed image interpretation, and the elimination of the stream tunnel visible on the 90m DEM. Accuracy varied from a low of 7% (3FDWRD at 90m, using a 10% threshold) to a high of 73% (2FD at 30m with a 20% threshold). Thus the

2FD method, while generating significant error, may yield good stream networks. Ironically the worst performing algorithm, SIMPLE D, also had accuracies of up to 59% (3m with a 20% threshold).

Table 11. Accuracy Statistics for Stream Recognition

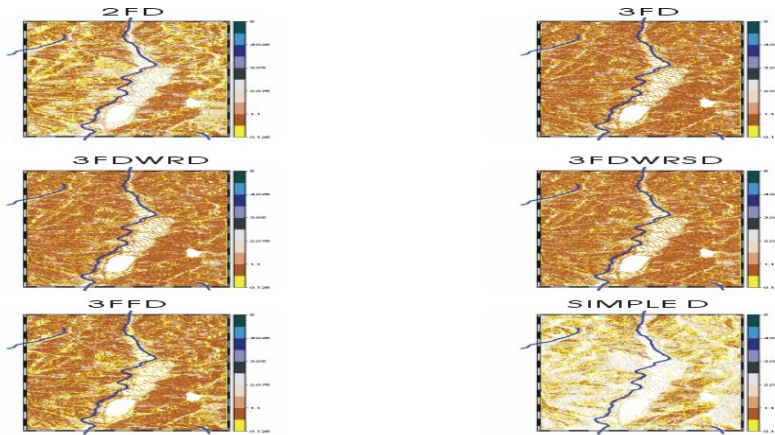


Conclusions

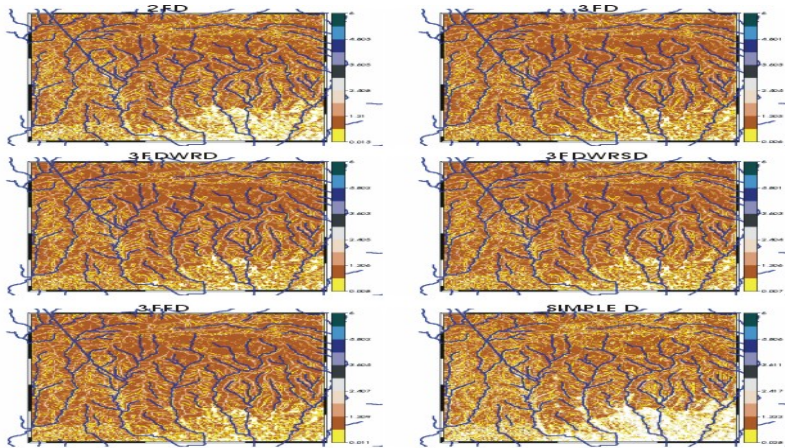
According to the results, the 3FD, 3FDWRD, 3FDWRS D, and 3FFD algorithms at most resolutions have similar characteristics to each other in all the cases (except for the down slope accumulation parameters at 30m and 90m at the 20% threshold) In this final result, the 2FD and SIMPLE D algorithms created far more overlay area than the others, resulting in apparent but not necessarily repeatable high accuracies.

There are statistically significant differences between the fundamental topographic parameter, slope, aspect, curvature, and down slope among all six methods. From all of these results, the result calculated for slope and aspect shows that the 3FDWRD algorithm gives comparatively the most precise results. The 3FD, 3FDWRS D, and 3FFD algorithms have very similar results with 3FDWRD. The SIMPLE D algorithm shows by far the greatest differences when comparing among the algorithms. This algorithm is apparently unique because SIMPLE D uses only a 2 pixel neighborhood to calculate the fundamental topographic parameter. It is interesting that the SIMPLE D assessed accuracies are high in every resolution and method, but this may be due to overestimation of stream area.

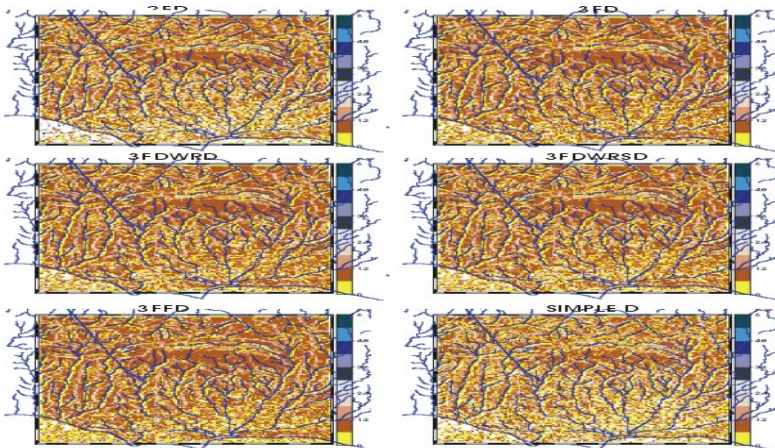
As a summary recommendation, the 3FDWRD algorithm is preferred in all instances, it yields a more precise result, and over a wide range of values. In this study, we have investigated the difference between six algorithms. In future work, we hope to both give a more complete set of results, and to further investigate the inter-relations of the fundamental topographic parameters.



3m DEM



30m DEM



90m DEM

Figure 9. Digitized flow line and assessed accumulation at the 3 resolutions

References

- Carter, J., (1992). The Effect of Data Precision On The Calculation Of Slope And Aspect Using Gridded DEMs. *Cartographica*, Vol. 29, No. 1, p. 22-34..
- Chu, T.H. and T.H. Tsai., (1995). Comparison of accuracy and algorithms of slope and aspect measures from DEM, in *Proceedings of GIS AM/FM ASIA '95*, p. 21-24 August, Bangkok.
- Costa-Cabral, M., and Burgess, S., (1994). Digital Elevation Model Networks (DEMON): A model of flow over hillslopes for computation of contributing and dispersal areas. *Water Resources Research*, Vol. 30, No. 6, p. 1681-1692.
- Douglas, D.H., (1986). Experiments to locate ridges and channels to create a new type of digital elevation model. *Cartographica* Vol. 23, p. 29-61.
- Evans, I.S., (1980). An integrated system of terrain analysis and slope mapping, *Zeitschrift fur Geomorphologie*, Supplement Band, Vol. 36, p.274-295.
- Evans, I.S., (1998). What Do Terrain Statistics Really Mean?. In: *Landform Monitoring, Modelling and Analysis*, Edited by S. N. Lane, K. S. Richards and J. H. Chandler, John Wiley and Sons, 300 pp.
- Fleming, M.D., and R.M. Hoffer., (1979). Machine processing of Landsat MSS data and LARS Technical Report 062879, Laboratory for Applications of Remote Sensing, Purdue University, West Lafayette, Indiana.
- Gallant, J.C. and Wilson, J. P., (1996). TAPES-G: A Grid-Based Terrain Analysis Program for the Environmental Sciences, *Computer & Geosciences*, Vol. 22, No. 7, p. 713-722.
- Horn, B.K.P., (1981). Hill shading and the reflectance map, *Proceedings of IEEE*, Vol. 69, No. 1, p. 14-47.
- Hunter, G. and Goodchild, M., (1997). Modeling the Uncertainty of Slope and Aspect Estimates Derived From Spatial Databases. *Geographical Analysis*, Vol. 29, No. 1, p. 35-49.
- Hutchinson, M. F., (1989) A New Procedure for Gridding Elevation and Stream Line Data With Automatic Removal of Pits. *Journal of Hydrology*, Vol. 106, p. 211-232.
- Jenson, S. and Domingue, J., (1988). Extracting Topographic Structure from Digital Elevation Data for Geographic Information System Analysis. *Photogrammetric Engineering and Remote Sensing*, Vol. 54, No. 11, p. 1593-1600.
- Jones, K.H., (1988). A comparison of algorithms used to compute hill slope as a property of the DEM, *Computer and Geosciences*, Vol. 24, No. 4, p. 315-323.
- Lee, J., (1996). Digital Elevation Models: Issues of Data Accuracy and Applications. ESRI User Conference, www.esri.com/resources/userconf/proc96.
- Lee, J., Snyder, P., and Fisher, P., (1992). Modeling the Effect of Data Errors on Feature Extraction From Digital Elevation Models. *Photogrammetric Engineering and Remote Sensing*, Vol. 58, No. 10, p. 1461-1467.
- Lea Nicholas J., (1992). An aspect-driven kinematic routing algorithm, in *Over Land Flow: Hydraulics and Erosion mechanics*, edited by A.J. Parsons and A.D. Abrahams, . Chapman and Hall, p. 393-407.
- Moore, I. D., Gessler, P. E., Nielsen, G. A., and Peterson, G. A., (1993). Soil attribute prediction using terrain analysis. *Soil Science Society of America Journal*, Vol. 57, p. 443-455.
- Moore, I. D., Grayson, R. B. and Ladson, A. R., (1991) Digital terrain modeling: A review of hydrological, geomorphological, and ecological applications. *Hydrological Processes*, Vol. 5, p. 3-30.

- O'Callaghan, J.F. and Mark, D.M., (1984). The extraction of drainage networks from digital elevation data, *Computer vision, Graphics and Image Processing*, Vol. 28, p. 323-344.
- Quinn, P., Beven, K., and Lamb, R., (1995). The $\ln(A/\tan B)$ index: How to calculate it and how to use it within the Topmodel framework. *Hydrological Processes*, Vol. 9, p. 1611-182.
- Quinn, P., Beven, K., Chevallier, P. and Plancon, O., (1991). The prediction of hillslope flow paths for distributed hydrological modeling using digital terrain models. *Hydrological Processes*, Vol. 5, p. 59-79.
- Reiger, W., (1998) A Phenomenon-Based Approach to Upslope Contributing Areas and Depressions in DEMs. *Hydrological Processes*, Vol. 12, p. 857-872.
- Ritter, D., (1987) A vector-based slope and aspect generation algorithm, *Photogrammetric Engineering & Remote Sensing*, Vol. 53, No. 8, p. 857-872.
- Ryder, W. and Voyadgis, D., (1996). Measuring the Performance of Algorithms for Generating Ground Slope. p. 208-216, In: *Spatial Accuracy Assessment in Natural Resources and Environmental Sciences: Second International Symposium*, United States Department of Agriculture, Rocky Mountain Forest and Range Experiment Station, Fort Collins, CO, Report RM-GTR-277.
- Salzmann, N., Kaab, A., Huggel, C., Allgower, B and Haeberli, W., (2004). Assessment of the Hazard Potential of Ice Avalanches using remote sensing and GIS-modelling. *Norsk Geografisk Tidsskrift-Norwegian Journal of Geography*, Vol. 58, p. 74-84.
- Sharpnack, D.A., and G. Akin., (1969). An Algorithm for computing slope and aspect from elevation, *Photogrammetric Survey*, Vol. 35, p. 247-248.
- Speight, J.G., (1974).A parametric approach to landform regions. In E.H. Brown and R.S Waters(eds.), *Progress in Geomorphology*. London: Alden, p. 213-230.
- Speight, J.G., (1980).The role of topography in controlling throughflow generation: a discussion. *Earth Surface Processes*, Vol. 5, p. 187-191.
- Tarboton, D., (1997). A new method for the determination of flow directions and upslope areas in grid digital elevation models. *Water Resources Research*, Vol. 33, No. 2, p. 309-319.
- Tarboton, D., Bras, R., and Rodriguez-Iturbe, I. (1993). On the extraction of channel networks from digital elevation data. In: *Terrain Analysis and Distributed Modeling In Hydrology*, Edited By: K. Beven, I.D. Moore, John Wiley and Sons, New York, NY, p. 85-104.
- Tobler, W. (1967), "Of Maps and Matrices," *Journal of Regional Science*, Vol. 7, p. 275-280.
- Unwin, D., (1981). *Introductory Spatial Analysis*. Methuen, London and New York.
- Wolock, D. and McCabe, G., (1995). Comparison of single and multiple flow direction algorithms for computing topographic parameters. *Water Resources Research*, Vol. 31, No. 5, p. 1315-1324.
- Wood, J.D., (1996). *The Geomorphological Characterization of Digital Elevation Model*, PhD Thesis, University of Leicester.
- Wilson, J. P. and John C. Gallant., (2000). *Terrain Analysis. Principles and Applications*. New York: J. Wiley.
- Zevenbergen, L.W., and C.R. Throne., (1987). Quantitative analysis of land surface topography. *Earth Surface processes and Landforms.*,Vol.12, p. 47-56.
- Zhou, Q. and X. Liu., (2002). Error assessment of grid-based flow routing algorithms used in hydrological models, *International Journal of Geographical Information Science*, Vol.16, No. 8, p. 819-842.
- Zhou, Q. and X. Liu., (2002). Error analysis on grid-based slope and aspect algorithms, *Photogrammetric Engineering & Remote Sensing*, Vol. 70, No. 8, p. 957-962.